



LAWRENCE
LIVERMORE
NATIONAL
LABORATORY

ZnS and ZnSe immersion gratings for astronomical high-resolution spectroscopy - evaluation of internal attenuation of bulk materials in the short NIR region

Y. Ikeda, N. Kobayashi, S. Kondo, C. Yasui, P. J. Kuzmenko, H. Tokoro, H. Terada

August 21, 2009

Optical Engineering

Disclaimer

This document was prepared as an account of work sponsored by an agency of the United States government. Neither the United States government nor Lawrence Livermore National Security, LLC, nor any of their employees makes any warranty, expressed or implied, or assumes any legal liability or responsibility for the accuracy, completeness, or usefulness of any information, apparatus, product, or process disclosed, or represents that its use would not infringe privately owned rights. Reference herein to any specific commercial product, process, or service by trade name, trademark, manufacturer, or otherwise does not necessarily constitute or imply its endorsement, recommendation, or favoring by the United States government or Lawrence Livermore National Security, LLC. The views and opinions of authors expressed herein do not necessarily state or reflect those of the United States government or Lawrence Livermore National Security, LLC, and shall not be used for advertising or product endorsement purposes.

ZnS and ZnSe Immersion Gratings for Astronomical High-resolution Spectroscopy — Evaluation of internal attenuation of bulk materials in the short NIR region

Yuji Ikeda

*Photocoding, 3-16-8-101 Higashi-Hashimoto, Sagami-hara, Kanagawa 229-1104 Japan**

Naoto Kobayashi, Sohei Kondo, and Chikako Yasui

Institute of Astronomy, University of Tokyo, 2-21-1 Osawa, Mitaka, Tokyo 181-0015 Japan

Paul J. Kuzmenko

Lawrence Livermore National Laboratory, 7000 East Avenue, Livermore, CA 94550, U.S.A.

Hitoshi Tokoro

Nano-Optonics Research Institute, Inc., 1333-1 Atobe, Mugegawa, Seki, Gifu 501-2697 Japan

Hiroshi Terada

Subaru Telescope, 650 North A'ohoku Place, Hilo, HI 96720 U.S.A.

We measure the internal attenuation of bulk crystals of CVD-ZnS, CVD-ZnSe, Si, and GaAs, in the short near-infrared (sNIR) region to evaluate the possibility of astronomical immersion gratings with those high refractive index materials. We confirm that multispectral grade CVD-ZnS and CVD-ZnSe are best suited for the immersion gratings, with the smallest internal attenuation of $\alpha_{\text{att}} = 0.01 - 0.03 \text{ cm}^{-1}$ among the major candidates. The measured attenuation is roughly in proportion to λ^{-2} , suggesting it is dominated by bulk scattering due to the polycrystalline grains rather than by absorption. The total transmittance in the immersion grating is estimated to be at least $> 80 \%$, even for the spectral resolution of $R = 300,000$. Two potential problems, the scattered light by the bulk material and the degradation of the spectral resolution due to the gradient illumination in the diffracted beam, are investigated and found to be negligible for usual astronomical applications. Since the remaining problem, the difficulty of cutting grooves on CVD-ZnS and CVD-ZnSe, has recently been overcome by the nanoprecision fly-cutting technique, ZnS and ZnSe immersion gratings for astronomy can be technically realized.

PACS numbers: Valid PACS appear here

I. INTRODUCTION

A. Immersion grating

Immersion grating is a powerful enabling technology for high-resolution spectroscopy in which the grooved surface is immersed in an optical material with the refractive index n (see Fig.1). As is well known, the theoretical spectral resolution of an immersed reflective echelle grating (R) is given by

$$R \equiv \frac{\lambda}{\Delta\lambda}, \quad (1)$$

$$= Nm, \quad (2)$$

$$= \frac{2n\phi \tan \theta}{\lambda}, \quad (3)$$

under the Littrow condition, where N and m are the number of the grooves and diffraction order, ϕ is the diameter of the collimated beam in the spectrometer, θ is the blaze angle, and λ is the wavelength. This equa-

tion suggests that immersion grating can provide n times higher resolution or a more compact ($1/n$) spectrometer than using a classical reflective grating whose diffraction surface is in the air ($n = 1$). As far as we know, Hulthén & Heuhaus (1954) are the first to mention and demonstrate the potential of immersion grating [1]. Since this, the theoretical performance of immersion grating has been discussed in detail [2–5]. However, there has been little practical immersion gratings except for a BK7 immersion grating in Ref.[6] and a silicon immersion grating in Ref.[7] because of the difficulty of the fabrication.

B. Astronomical application of immersion grating

High-resolution spectroscopy of $R \geq 100,000$ in the near infrared (NIR: $\lambda > 0.9 \mu\text{m}$) is beginning to attract attention in the fields of astronomy and astrophysics. In the visible region, numerous high resolution spectra with $R \geq 100,000$ have been obtained by spectrographs, attached to 8 – 10 m class telescopes, which employ classical reflective echelle gratings (e.g., HIRES at Keck [8], UVES at VLT [9], and HDS at Subaru [10]). However, there have been few spectrographs for the NIR regions, except for the latest instrument CRIRES mounted on

*Electronic address: ikeda@photocoding.com

VLT [11]. This is because not only does the collimated beam, and therefore the instrumental volume, becomes much larger than that for the visible in proportion to the wavelength (see Eq.(3)), but also the whole instrument must often be cooled to cryogenic temperatures. These requirements result in extensive engineering design, requiring much more time and budget for development.

Because IR-transmitting semiconductor materials often have a higher refractive index of $n > 2$ than typical optical glasses and chemical crystals, immersion gratings using these materials may overcome the prior problem by realizing a more compact NIR high-resolution spectrograph. Dekker proposed the possibility of applying this technique to astronomical high-resolution spectrographs for the first time [12]. Wiedemann et al. (1993) suggest that immersion gratings could have great benefits in the infrared region [13]. They propose fabrication by chemical etching of single crystal silicon and germanium, which transmit at longer NIR, $\lambda > 1.3 \mu\text{m}$ and $\lambda > 2.0 \mu\text{m}$, respectively. Recently, Marsh et al. (2007) finally succeeded in developing a practical silicon immersion grating with high efficiency by photolithographic etching [7].

However, we have only immersion gratings for the long NIR now. As a natural extension, it is desirable to extend the wavelength coverage to the short NIR region (sNIR; $0.9 - 1.3 \mu\text{m}$). The sNIR region also has not been fully exploited as "niche" bands from the viewpoint of technology because it has been out of the sensitivity range of both CCD and infrared array detectors, although there are many important atomic/molecular lines from various astronomical objects. In the age of the next generation extremely large telescopes (ELT, Refs.[14–16]), the sNIR spectrographs with even higher spectral resolution will be naturally required to exploit the high photon gathering power. Therefore, the requests for high-resolution spectrographs for the sNIR using immersion gratings, providing a compact ($1/n$) spectrograph, will be increasing, because the instruments for ELTs must be large proportional to the telescope diameters under the natural seeing condition (see Eq.(11) in sect.III B). However, many IR transmission materials are not usable as immersion grating for the sNIR, because they often absorb the NIR and visible lights and because the methods of machining fine grooves are not always established for all materials (the optical glasses, which transmit these wavelengths, are inadequate because thick glasses with the high indices ($n > 2$) have not been realized yet). Therefore, we must first begin to search and select suitable materials for fulfilling these next astronomical requirements.

C. Candidate material

Fig.2 summarizes the NIR absorption coefficients α_{abs} [cm^{-1}] of available semiconducting materials, gathered from various literature and catalogues. Silicon and germanium are obviously good materials only for the long NIR region ($\lambda > 2 \mu\text{m}$). GaP shows low absorption

through the NIR region. However, because the absorption gradually increases with the shorter wavelengths less than $1 \mu\text{m}$, it is a good candidate for a small (thin) grating, but might not be suitable for a large (thick) grating providing high spectral resolution in the sNIR region [39]. CdTe and GaAs are good materials for the long NIR region, but do not appear to be usable in the sNIR region in view of the large α_{abs} at $\lambda \sim 0.9 \mu\text{m}$. ZnS and ZnSe are the remaining good candidates because of very small α_{abs} through the entire sNIR region. However, even a tiny absorption coefficient may cause significant attenuation since high resolution immersion gratings require very thick material ($> 100 \text{ mm}$) to obtain a large optical path difference (see Fig.1). Moreover, because the large sizes of ZnS and ZnSe that are commercially available are polycrystalline, bulk scattering could contribute to the total attenuation. Therefore, it is very important to measure the attenuation with high precision by using thick ($> 10 \text{ mm}$) samples. The attenuation in the immersion grating could result in not only decreased total throughput, but also increased stray light and degraded spectral resolution. Those secondary effects should be carefully assessed before the development of immersion grating.

D. Goal

We present a new high-precision measurement of the attenuation of CVD-ZnS and CVD-ZnSe as well as Si and GaAs in the sNIR region. This research is a first step to realize the sNIR immersion grating.

Here we define an extended absorption coefficients as follows:

$$\alpha_{\text{att}} = \alpha_{\text{abs}} + \alpha_{\text{sca}}, \quad (4)$$

which shows the total attenuation including both the internal absorption (α_{abs}) and the bulk scattering (α_{sca}). The measurements of Si and GaAs are not intended to demonstrate utility as immersion gratings in the sNIR region, but to validate our measurement technique with data in the literature. From the results, we clarify the major origin of the attenuation for CVD-ZnS and CVD-ZnSe. Next, we discuss the effects of the measured attenuation to the total throughput, the stray light, and the spectral resolution of the spectrograph, when using CVD-ZnS and CVD-ZnSe for sNIR immersion grating. Finally, we comment on the possibility of fabricating gratings in those materials. With all of these considerations, we conclude that it is possible to fabricate an immersion grating for the sNIR region using CVD-ZnS and CVD-ZnSe.

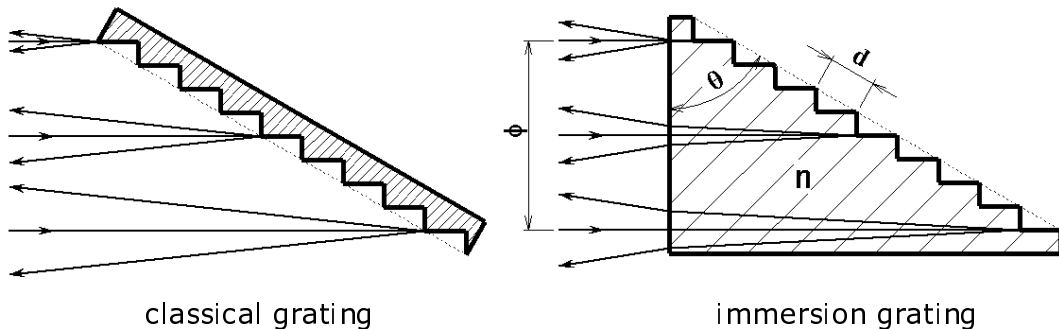


FIG. 1: Classical echelle grating and immersion grating

II. MEASUREMENTS OF INTERNAL ATTENUATION

A. Samples

For three materials (ZnS, ZnSe, and Si), we calculated the internal attenuation of the subject materials from the transmittances of two substrates with different thicknesses ($t = 5$ and 30 mm). By comparing the transmittance of the substrates, the loss due to surface reflection/scattering can be canceled out, and the pure internal attenuation can be obtained. Because GaAs is very expensive, we used a thin ($t = 0.385$ mm) substrate and calculated reflection losses from the known refractive index. The surface irregularities and parallelism are less than $\lambda/8$ at $0.633 \mu\text{m}$ and $3'$ for all the substrates. Therefore, there should be no significant difference in surface reflection between the 5 and 30 mm substrates of the same material.

Both ZnS and ZnSe substrates are polycrystalline made by CVD (= Chemical Vapor Deposition) method, and provided by II-VI Inc. in US. Practically only polycrystalline CVD-ZnS and CVD-ZnSe is available for immersion grating, because single crystal material is very difficult to grow, and little is available commercially. For ZnS, we used the “multispectral” grade, which transmits both visible and IR wavelengths. The Si substrates are single crystal, provided by Oyokoken-Kogyo Co., Ltd. in Japan. It is optical grade with a resistivity of $\geq 1 \times 10^3 \Omega \text{ cm}$. The GaAs substrate is a single crystal provided by Sumitomo Electric Industries, Ltd. in Japan, because only single crystal material is usually available for optical use at present. It is a normal optical grade with resistivity $\geq 1 \times 10^7 \Omega \text{ cm}$.

B. Method and measurement accuracy

For ZnSe, ZnS, and Si, the internal attenuation can be calculated using the following equation:

$$\alpha_{\text{att}} = -\frac{\ln [T_1/T_2]}{|t_1 - t_2|}, \quad (5)$$

where T_1 , t_1 and T_2 , t_2 are the measured transmittance and thickness for the thicker and thinner substrates, respectively. For GaAs, by accounting for all internal reflections, the internal attenuation is obtained by

$$\alpha_{\text{att}}^{\text{GaAs}} = \frac{1}{t_0} \ln \left[\frac{(1 - R_0)^2}{2T_0} \left(1 + \sqrt{1 + \frac{4R_0^2 T_0^2}{(1 - R_0)^4}} \right) \right], \quad (6)$$

where t_0 is the thickness, T_0 is the measured transmittance, and R_0 is the surface reflection given by $R_0 = (n - 1)^2 / (n + 1)^2$. The refractive index $n(\lambda)$ is referred from Ref.[17].

Fig.3 shows the optical layout of a spectrophotometer for measuring the transmittance. This spectrometer is a commercial *Solid Spec 3700*, built by Shimadzu Corporation in Japan. It employs a double optical path for the objective sample and the reference. These paths can be quickly switched by a chopping mirror. The detector unit has an integrating sphere, which reduces the photometric errors caused by varying illumination on the detector with uneven surface sensitivity. The illumination can easily change because of variations in the aberration (primarily coma aberration) on the focal surface, that are produced by the shift of the pupil image by $\Delta f = \Delta t(1 - 1/n)$ when measuring substrates having the different thickness of Δt .

The final measurement accuracy of the internal attenuation $\Delta\alpha_{\text{att}}$ of ZnS, ZnSe, and Si was determined by the offset uncertainty (Δ) and the statistical uncertainty (σ). We estimated Δ by measuring the attenuation α_{att} of the well-controlled high-index optical glass, S-TIH6 ($n = 1.77$), supplied by OHARA Inc., using two substrates of 2 and 30 mm thicknesses and eq.(5). The difference between the measured attenuation and the cataloged attenuation (see <http://www.ohara-inc.co.jp/en/product/optical/list/index.html>) was set to Δ . The statistical error σ was estimated from the standard deviation for multiple measurements. We define the sum of $|\Delta|$ and σ ,

$$\sigma_{\alpha_{\text{att}}} = |\Delta| + \sigma, \quad (7)$$

as the final measurement uncertainty. In our work, $|\Delta|$ and σ are comparable in magnitude. Finally, the esti-

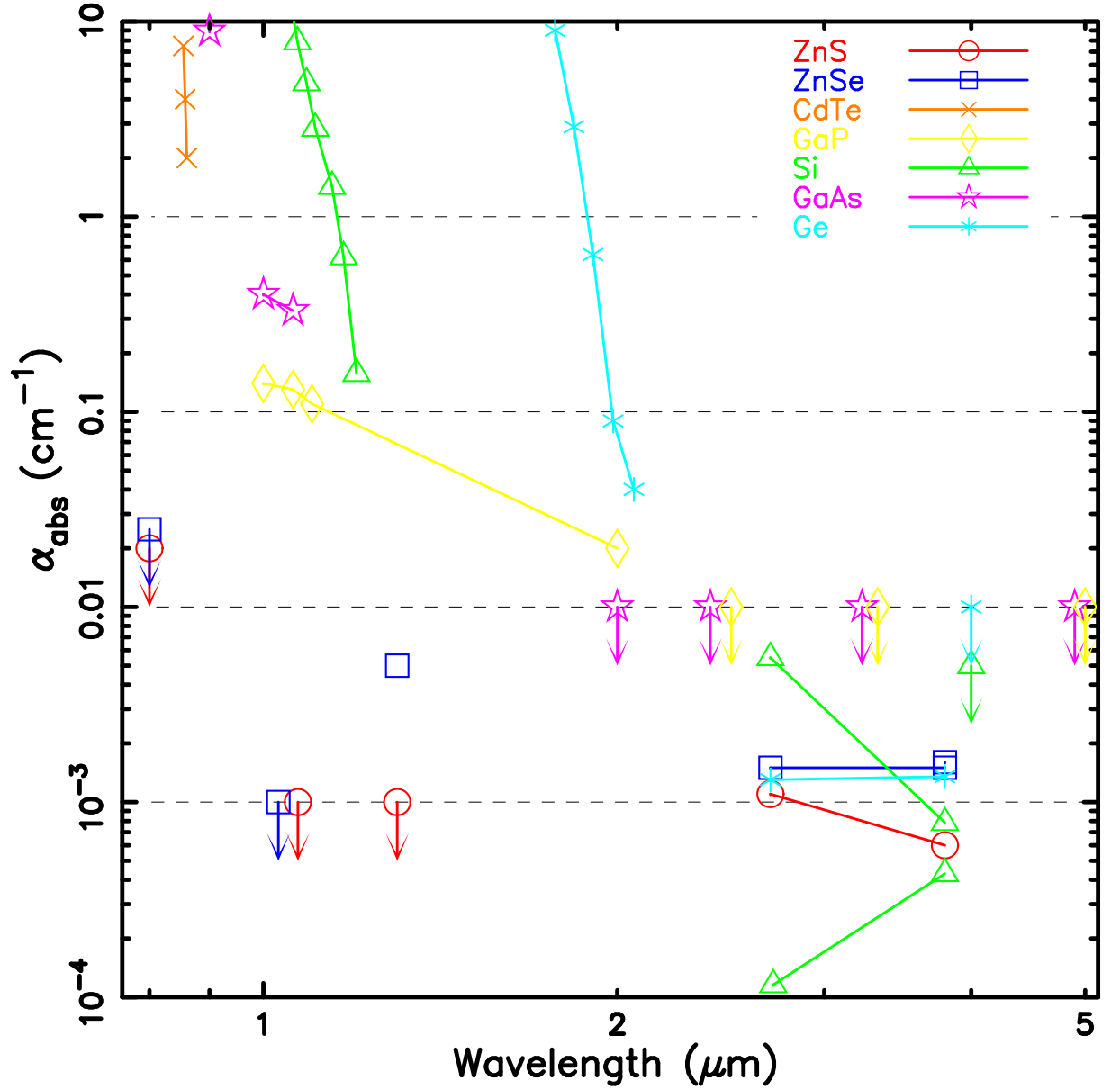


FIG. 2: The absorption coefficients α_{abs} of ZnS (red open-circles), ZnSe (blue open-squares), CdTe (orange crosses), GaP (yellow open-diamonds), Si (green open-triangles), GaAs (violet open-stars), and Ge (turquoise asterisks) in the NIR region. The references are as follows; ZnS: Ref.[17] and the unpublished data from the II-VI Inc., ZnSe: Refs.[18, 19] and the unpublished data from the II-VI Inc., CdTe: Ref.[20], GaP: Ref.[21], Si: Refs.[17, 22, 23], GaAs: Refs.[21, 24], and Ge: Refs.[17, 25, 26]. Data points of ZnSe at $1.07 \mu\text{m}$ and GaAs at $2.50 \mu\text{m}$, $3.33 \mu\text{m}$ and $5.00 \mu\text{m}$ are shifted to the left by $0.04 \mu\text{m}$ and $0.1 \mu\text{m}$ for viewing purpose, respectively.

mated uncertainties are $\sigma_{\alpha_{\text{att}}} = 0.7 \times 10^{-3} \text{ cm}^{-1}$ at $0.8 \mu\text{m}$, $\sigma_{\alpha_{\text{att}}} = 0.6 \times 10^{-3} \text{ cm}^{-1}$ at $1.0 \mu\text{m}$, $\sigma_{\alpha_{\text{att}}} = 0.4 \times 10^{-3} \text{ cm}^{-1}$ at $1.2 \mu\text{m}$, and $\sigma_{\alpha_{\text{att}}} = 2.9 \times 10^{-3} \text{ cm}^{-1}$ at $1.4 \mu\text{m}$. These values are less than the required accuracy, proving the high-accuracy of our measurement using two substrates. However, the uncertainties around $\lambda = 0.9 \mu\text{m}$ are worse than previous mentioned. This is because the gratings of the monochromator are changed at this wavelength and the output signals became unstable (see Fig.4 and Tab.I). As shown in the next section, the internal at-

tenuation of Si was measured at about $1.0 \times 10^{-3} \text{ cm}^{-1}$ at $1.3 - 1.5 \mu\text{m}$. They are consistent with the published absorption coefficients in longer wavelengths ($\lambda > 2 \mu\text{m}$) in Fig.2 within the estimated uncertainty, confirming the consistency of our measurement.

For GaAs, the accuracy was directly determined from the photometric uncertainty of the spectrophotometer ($\Delta T_0 \sim 0.3 \%$) and eq.(6) to be $\sigma_{\alpha_{\text{att}}} = 8.8 \times 10^{-2} \text{ cm}^{-1}$ over the wavelength range of measurement. The accuracy is about two orders of magnitude worse than that

from the measurement with two substrates.

C. Results

Fig.4 and Tab.I summarize the obtained internal attenuation. The detail of the results for each material is discussed in the following sections.

1. ZnS and ZnSe

The CVD-ZnS (multispectral grade) and CVD-ZnSe show low attenuation ($0.01 - 0.03 \text{ cm}^{-1}$) in the measured wavelength range. The attenuation of ZnS becomes less than that of ZnSe at shorter wavelengths. The red open-circles and blue open-squares in Fig.4 show the absorption coefficients σ_{abs} for CVD-ZnS and CVD-ZnSe, respectively, that are privately provided by II-VI Inc. They are much smaller than our measured attenuation. The absorption coefficients by II-VI show pure internal absorption obtained by the laser calorimetry method (see Ref.[27]).

2. Si

Single crystal Si shows an extremely low attenuation of $\leq 0.001 \text{ cm}^{-1}$ at $\lambda \geq 1.26 \mu\text{m}$, while the attenuation steeply increases with decreasing wavelength from $1.2 \mu\text{m}$. Ref.[28] reports the pure absorption coefficients at longer wavelengths, $\sigma_{\text{abs}} = 1.16 \times 10^{-4} \text{ cm}^{-1}$ at $2.7 \mu\text{m}$ and $\sigma_{\text{abs}} = 4.30 \times 10^{-4} \text{ cm}^{-1}$ at $3.8 \mu\text{m}$, which are consistent with our results. At the short wavelength absorption edge around $1.2 \mu\text{m}$, our data and the data in the literature appear to be discontinuous, which may be due to the difference of the resistivity, namely the amount of impurities. the resistivity of silicon reported in the literature is $100 \Omega \text{ cm}$ [29], which is much smaller than that of our sample ($> 1 \times 10^3 \Omega \text{ cm}$). Ref.[30] experimentally shows that the absorption edges differ between several samples with the difference of the resistivities.

3. GaAs

Single crystal GaAs shows a large attenuation at $\lambda < 1.0 \mu\text{m}$ and a slowly decreasing attenuation with increasing wavelength. However, the attenuation is still $\sim 0.1 \text{ cm}^{-1}$ at $1.3 \mu\text{m}$. Our results are in good agreement with Ref.[24] at $0.9 \mu\text{m}$, but are not in agreement with those of Ref.[21] at 1.0 and $1.06 \mu\text{m}$. This may be caused by the difference of the impurity due to the difference of their growth methods. While our GaAs is a single crystal grown by the vertical Bridgeman (VB) method, which is more commonly used for commercial production, the GaAs in [21] is a polycrystal grown by the compound-gradient freeze process. We did not show the data

at $\lambda > 1.3 \mu\text{m}$, because the uncertainty $\sigma_{\alpha_{\text{att}}}$ for GaAs is significantly larger than the attenuation in this longer wavelength region.

III. DISCUSSION

A. Internal absorption and bulk scattering

Our measured attenuation of CVD-ZnS and CVD-ZnSe are an order of magnitude higher than the pure internal absorption measured by II-IV Inc (Fig.4). This suggests that the attenuation in the sNIR region is dominated by bulk scattering, which can be naturally attributed to the polycrystalline nature of the materials. By contrast, the attenuation of single crystal Si and GaAs is similar to the absorption coefficients in the literature: the bulk scattering of those materials appears to be negligible in the NIR region.

The bulk scattering of polycrystalline materials is thought to be attributed to the perturbation of a wavefront by the inhomogeneous spatial/size distributions of the small polycrystalline grains. As described in various basic text books on optics (e.g., Ref.[31]), the intensity of scattered light by randomly small fluctuations is proportional to λ^{-2} . The slopes of ZnS and ZnSe data points can be well approximated by λ^{-2} line (see the solid line in Fig.4), which strongly supports that the attenuation of CVD-ZnS and ZnSe is dominated by the bulk scattering attributed to the polycrystalline nature in the sNIR region.

B. Throughput of an immersion grating

In general, total throughput of an immersion grating η_{tot} can be written as

$$\eta_{\text{tot}} = \eta_{\text{diff}} \times \eta_{\text{sur}}^2 \times \eta_{\text{att}}, \quad (8)$$

where η_{diff} is the absolute diffraction efficiency of the groove surface, η_{sur} is the transmittance at the entrance or the exit surface, and the η_{att} is the transmittance of the bulk material. The preferable efficiency values are $\eta_{\text{diff}} \geq 0.7$, $\eta_{\text{sur}} \geq 0.95$, and $\eta_{\text{att}} \geq 0.9$ for general astronomical applications.

For a simple model (Fig.5), the transmittance η_{att} can be written as

$$\eta_{\text{att}} = \frac{2}{\pi a^2} \int_0^{2a} \sqrt{2a - x^2} \exp[-2\alpha_{\text{att}}(\lambda)x \tan \theta] dx, \quad (9)$$

where $2a$ is the beam diameter. With a non-dimensional aperture size $t \equiv x/a$ and Eq.(3), Eq.(9) can be rewritten as

$$\eta_{\text{att}}(R, \lambda) = \frac{2}{\pi} \int_0^2 \sqrt{2t - t^2} \exp\left[-\frac{\alpha_{\text{att}}(\lambda)R\lambda_0}{2n}t\right] dt, \quad (10)$$

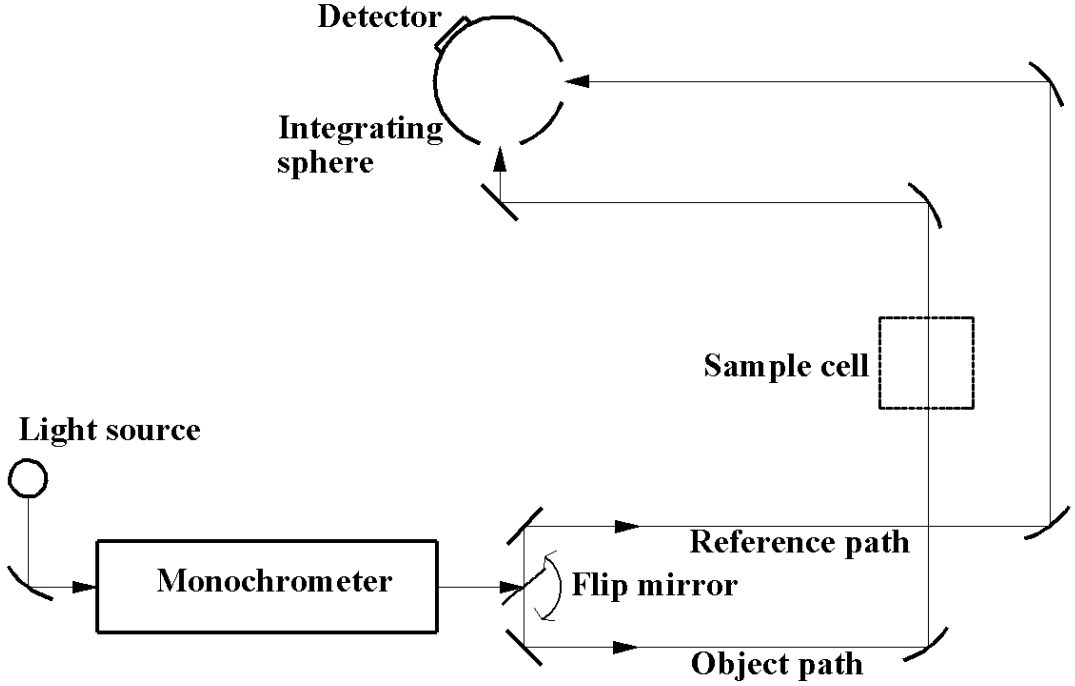


FIG. 3: Optical layout of the spectrophotometer. The quasi-monochromatic light produced by the monochromator is divided into two beams for the object and the reference by the flip-mirror. Both beams are led into the same integrating sphere with a photo-detector. For simplicity, some fold mirrors actually present in the spectrometer are omitted in this figure.

where λ_0 is the principal wavelength to define the spectral resolution. Note that η_{att} is determined by only two parameters, the internal attenuation σ_{att} and the spectral resolution R .

Fig.6 shows calculated η_{att} of ZnS and ZnSe for three spectral resolutions, $R = 100,000$, $200,000$, and $300,000$ at $\lambda_0 = 1.0 \mu\text{m}$. The base length of the triangle prism is 21.8, 43.6, and 65.4 mm for ZnS, and 20.1, 40.2, and 60.3 mm for ZnSe, respectively. For $R = 100,000$ and $R = 200,000$, η_{att} is sufficiently high (≥ 0.9) in the overall wavelengths of $0.9 - 1.5 \mu\text{m}$. For $R = 300,000$, the attenuation is not negligible for the shorter wavelengths of less than $1.1 \mu\text{m}$. Thus, the high efficiency immersion grating with $R \leq 200,000$ is easily possible using CVD-ZnS or CVD-ZnSe. However, we should pay attention to the internal attenuation when using an immersion grating with $R \geq 300,000$, particularly at less than $1.1 \mu\text{m}$.

For an astronomical spectrograph, we should account for the seeing effect. The entrance slit width s must be designed to fit to the seeing size rather than the spot size of the diffraction limited PSF. In this case, the spectral resolution given by Eq.(3) is modified as follows,

$$R_{\text{slit}} = \frac{2n\phi \tan \theta}{Ds}, \quad (11)$$

where D is the entrance pupil diameter of the telescope. Because s is greater than λ/D for the ground-based observations under the seeing-limited conditions, much thicker bulk materials are required to maintain the high

spectral resolution, resulting in larger internal attenuation (by a factor under typical observing conditions) than those shown in Fig.6.

Mosaic immersion grating (Fig.7) recovers the throughput for ground-based observations to the level as shown in Fig.6. It has a few small (thin) immersion gratings aligned in the collimated beam, which reduces the internal attenuation due to the thick materials. The size of each small immersion grating should be determined as the theoretical spectral resolution (R) by Eq.(3) becomes higher than the actual spectral resolution (R_{slit}) determined by the slit width. Thus, even though we use the small immersion gratings, the spectral resolution is not degraded compared to that of a spectrograph with a large single immersion grating. This mosaic immersion grating has an advantage in fabrication and cost because of use of only a small ingot. However, we should take care of the inevitable energy loss around the boundaries between small immersion gratings. Alternatively, the use of adaptive optics (AO, e.g., Ref.[32]) recovers the throughput, because AO improves the wavefront aberrations (the seeing size) and therefore the size of the immersion grating.

C. Background scattered light

Because the internal attenuation of the CVD-ZnS and CVD-ZnSe bulk material is dominated by the bulk scattering, it could become a significant background noise

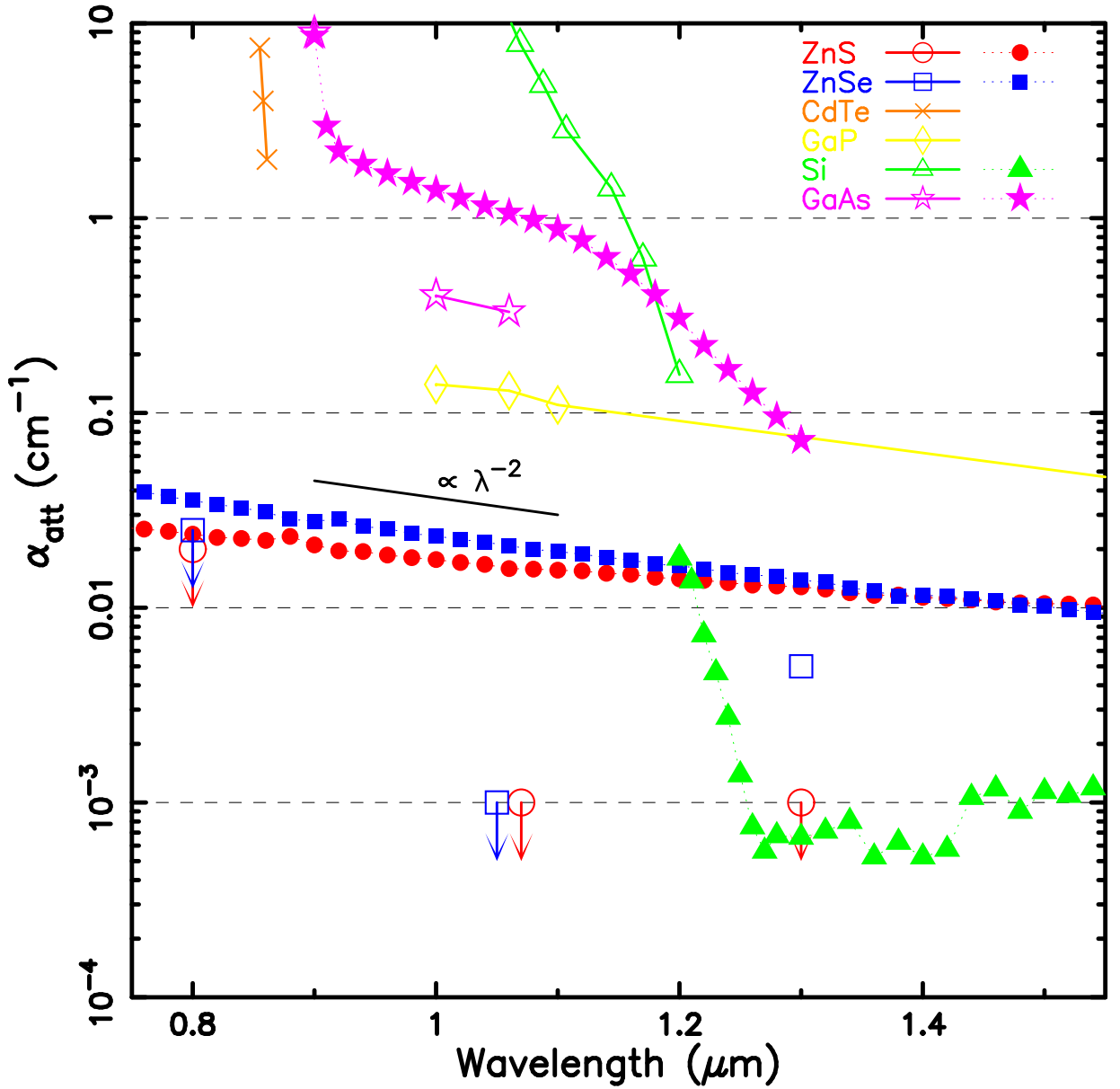


FIG. 4: Measured internal attenuation α_{att} of CVD-ZnS, CVD-ZnSe, Si, and GaAs between 0.8 – 1.5 μm . The red filled-circles (for CVD-ZnS), the blue filled-squares (for CVD-ZnSe), the green filled-triangles (for Si), and the violet filled-stars (for GaAs) show the attenuation from this work. The other marks are absorption coefficients from the literature or private communication already shown in Fig.2. A data point of ZnSe at 1.07 μm is slightly shifted to the right by 0.01 μm for viewing purpose.

source on the detector. In the laboratory, a faint but clearly visible scattered light from the ZnSe block was observed when it was exposed to the He-Ne laser beam. Although the scattering should be negligible in the longer wavelengths such as the sNIR region, here we estimated the effect of the bulk scattering with some simple assumptions. Because α_{att} is very small, the total opacity of the beam through the bulk material ($\alpha_{\text{att}} \times L$, where L is an order of 100 mm) is much smaller than 1. Therefore, we can assume only single scattering in the bulk contributes to the total scattered flux, and the effect of multiple scattering is not considered in the following estimates.

The intensity of the scattered light in a small solid angle $\Delta\Omega$ is given by

$$I_{\text{sca}} = \frac{1}{4\pi} \frac{K(\beta) + K(-\beta)}{2} \Delta\Omega \int_{\lambda_{\min}}^{\lambda_{\max}} f(\lambda) [1 - \eta_{\text{sca}}(\lambda)] (d\lambda) \\ \leq \frac{1}{4\pi} \frac{K(\beta) + K(-\beta)}{2} \Delta\Omega \int_{\lambda_{\min}}^{\lambda_{\max}} f(\lambda) [1 - \eta_{\text{att}}(\lambda)] (d\lambda)$$

where η_{sca} is the bulk scattered component out of η_{att} , λ_{\max} and λ_{\min} are the maximum and minimum sensitive wavelengths of the spectrograph, $f(\lambda)$ is the spectral energy distribution of the target object including the sensi-

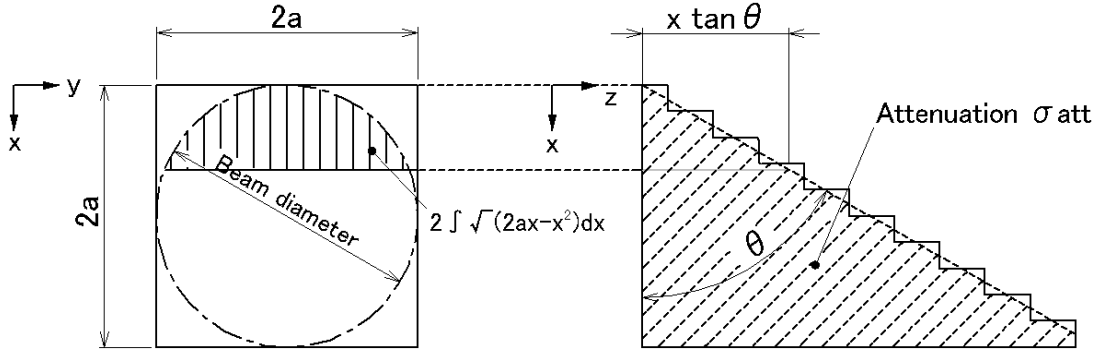


FIG. 5: A model sketch for the estimation of the internal attenuation loss in an immersion grating.

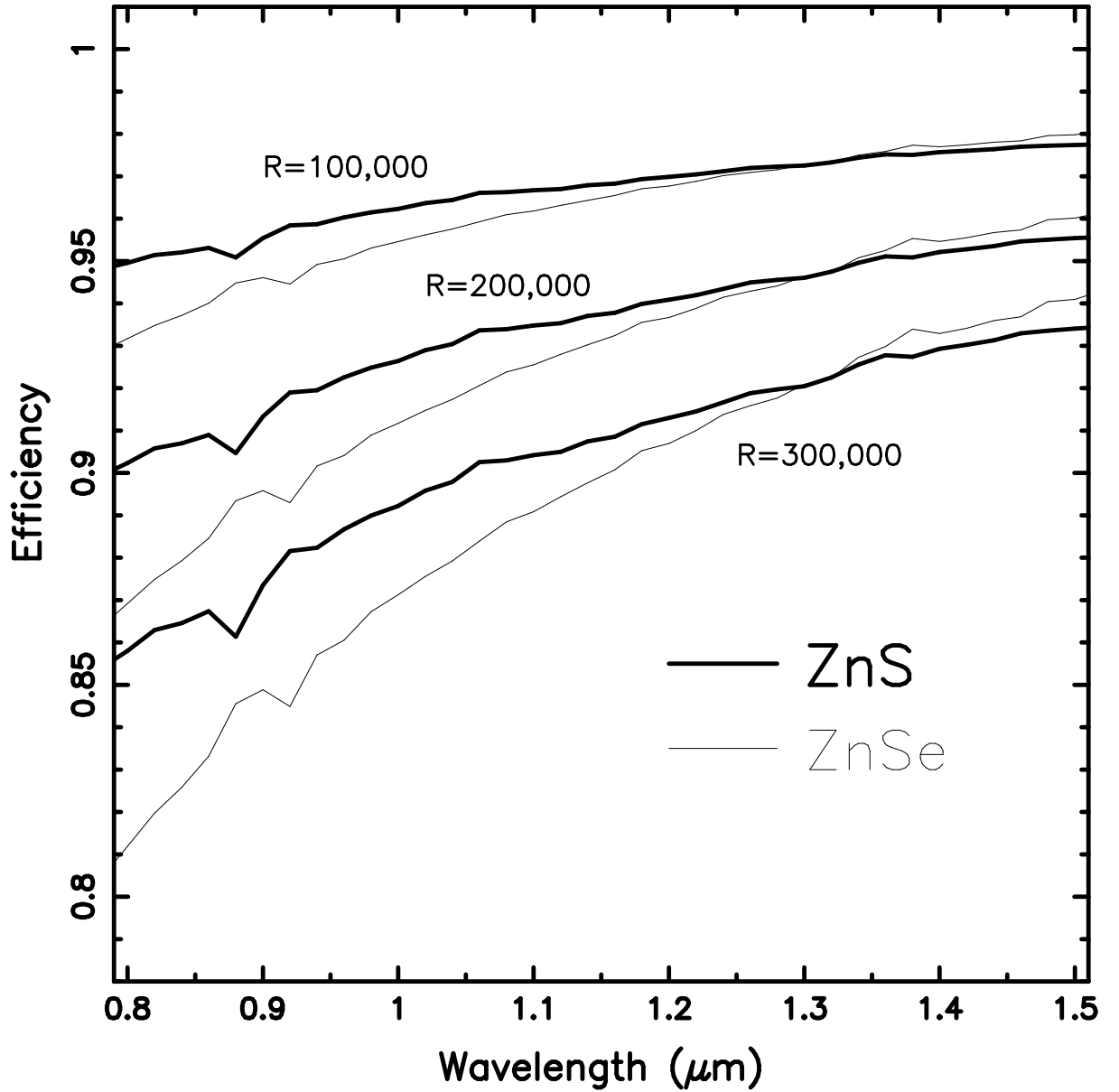
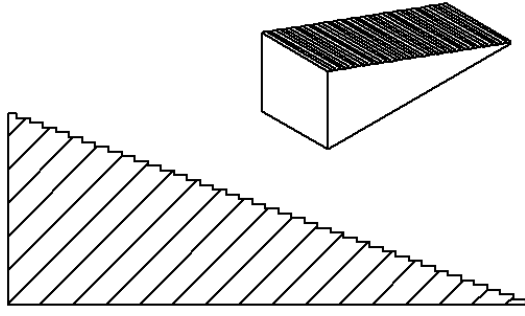
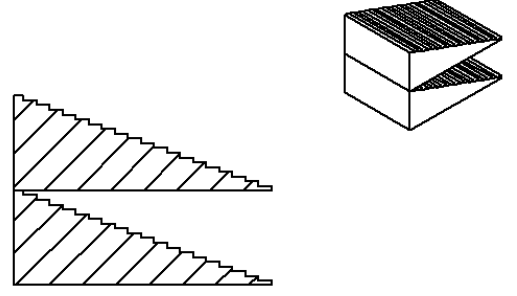


FIG. 6: The transmittance η_{att} of ZnS (solid lines) and ZnSe (thin lines) immersion gratings for the cases of $R = 100,000$, $200,000$, and $300,000$. The values around $0.9 \mu m$ are noisy because of the low measurement accuracy of α_{att} (see Sect.II B).



single immersion grating



mosaic immersion grating

FIG. 7: Schematics of a single immersion grating (left) and a mosaic immersion grating (right). Both gratings have the same clear aperture, but the latter has the shorter optical path (= thinner) than the former, resulting in significant improvement of the throughput (see text for more details).

tivity curve of the spectrograph, $K(\beta)$ is the phase function of the scattering, and β is the direction angle of the scattered light measured from the optical axis in the immersion grating. Under the Littrow condition, the small solid angle $\Delta\Omega$ can be written as

$$\Delta\Omega \simeq \pi\Delta\beta^2 \quad (14)$$

$$\simeq \pi \left(\frac{m\Delta\lambda}{nd\cos\theta} \right)^2, \quad (15)$$

$$\simeq \pi \left(\frac{2\tan\theta}{R} \right)^2, \quad (16)$$

where $\Delta\lambda$ is the monochromatic line width at λ_0 , R is the spectral resolution, and d and θ are the grating pitch and the blaze angle shown in Fig.1. Thus, the scattered light within $\Delta\lambda$ can be constrained as

$$I_{\text{sca}} \leq \frac{[K(\beta) + K(-\beta)] \tan^2 \theta}{2R^2} \int_{\lambda_{\min}}^{\lambda_{\max}} f(\lambda) [1 - \eta_{\text{sca}}(\lambda)] d\lambda. \quad (17)$$

On the other hand, since the intensity of the target object at λ_0 is,

$$I_0 = f(\lambda_0)\eta_{\text{att}}(\lambda_0)\Delta\lambda, \quad (18)$$

$$= \frac{f(\lambda_0)\eta_{\text{att}}(\lambda_0)\lambda_0}{R}, \quad (19)$$

the intensity ratio of the scattered light to the target object (γ) is given by,

$$\begin{aligned} \gamma &\equiv \frac{I_{\text{sca}}}{I_0} \\ &\leq \frac{[K(\beta) + K(-\beta)] \tan^2 \theta}{2f(\lambda_0)\eta_{\text{att}}(\lambda_0)R\lambda_0} \int_{\lambda_{\min}}^{\lambda_{\max}} f(\lambda) [1 - \eta_{\text{att}}(\lambda)] d\lambda \end{aligned} \quad (20)$$

Assuming an isotropic scattering ($K(\beta) = 1$) and a flat spectrum ($df/d\lambda = 0$) for simplicity, we finally obtain

$$\gamma \leq \frac{\tan^2 \theta}{R} \frac{(1 - \langle \eta_{\text{att}} \rangle)}{\eta_{\text{att}}(\lambda_0)} \frac{\lambda_{\max} - \lambda_{\min}}{\lambda_0}. \quad (22)$$

Note that the right side of Eq.(22) strongly depends on the blaze angle θ but no longer depends on the spectral resolution R , because $(1 - \langle \eta_{\text{att}} \rangle)$ is proportional to R for $\sigma_{\text{att}} \ll 1$ (see Eq.(10)). In the case of $\lambda_{\min} = 0.8 \mu\text{m}$, $\lambda_{\max} = 1.5 \mu\text{m}$, and $\lambda_0 = 1.0 \mu\text{m}$, the intensity ratio of the scattered light γ was estimated from Eq.(22) to be $\leq 7.8 \times 10^{-6}$ for ZnS and $\leq 8.9 \times 10^{-6}$ for ZnSe, respectively, for any combination of $\theta < 80$ degree and $R < 300,000$. Thus, scattering by the bulk material would be negligible for normal astronomical observations.

D. Degradation of spectral resolution

Because the attenuation in the immersion grating produces an axially asymmetric illumination in the collimated beam, the PSF on the focal plane is deformed. This could degrade the spectral resolution because the gradient of the illumination appears along the dispersion direction. We evaluated this effect by calculating the line spread functions (LSF) from the illumination gradient using the optical design software, CodeV. LSF is a cross section profile obtained by scanning a PSF along one direction, for example, the slit-length direction, and therefore it is equivalent to a monochromatic 1-D spectral line profile by observations. In case of a ZnSe immersion grating with $R = 300,000$, the calculated difference of the FWHM and $1/e^2$ width at $\lambda_0 = 1.0 \mu\text{m}$, between the hypothetical immersion grating with no attenuation and an actual immersion grating, is 0.05 and 0.08 %, respectively. Because this is an extreme case about the asymmetric illumination (see Fig.6), we conclude that the degradation of the spectral resolution by the attenuation is negligible.

E. Fabrication possibility

From the prior discussions, it is clear that ZnS and ZnSe immersion gratings are feasible. However, because both CVD-ZnS and CVD-ZnSe are soft brittle materials, it is difficult to cut fine grooves with extremely accurate pitch on these substrates.

Kuzmenko et al. suggest the possibility of the fabrication of ZnS and ZnSe gratings with a diamond-machining using a nanoprecision fly-cutting technique at the Lawrence Livermore National Laboratory [33]. They have succeeded fabrications of the good germanium immersion gratings with the same method [34, 35]. Recently, Kuzmenko et al. and Ikeda et al. machined a hundred grooves with a pitch of 30 μm and a blaze angle of 65 degree on a CVD-ZnSe substrate with this method, and reported that a good surface roughness and acceptable pitch errors were achieved [36, 37]. Moreover, they mentioned that immersion gratings by this technology show a high diffraction efficiency $\eta_{\text{diff}} > 80\%$ from the optical testing. In the near future, fabrication of the fine grooves on CVD-ZnS and CVD-ZnSe should become practical.

IV. SUMMARY

In astronomy, high resolution spectroscopy of $R \geq 100,000$ in the sNIR region ($0.9 - 1.3\ \mu\text{m}$) has begun to attract attention. Immersion grating is a practical solution for such requirements, because it can easily realize a compact high-resolution spectrograph. Among various IR-transmitting materials, ZnS and ZnSe are good candidates for immersion grating for this wavelength region because of high refractive indices and small absorption coefficients. However, because immersion grating requires thick bulk materials, even small attenuation could produce a serious energy loss and some secondary effects.

Thus, we conduct high-precision measurements of the

attenuation of CVD-ZnS and CVD-ZnSe as well as Si and GaAs in the sNIR region. CVD-ZnS and CVD-ZnSe are found to show the smallest internal attenuation of $\alpha_{\text{att}} = 0.01 - 0.03\ \text{cm}^{-1}$. With this attenuation, the total transmittance in the immersion grating is estimated to be $> 80\%$, even for $R = 300,000$. The background light scattered by the bulk material and the degradation of the spectral resolution due to a gradient illumination in the diffracted beam are investigated and found to be negligible for normal astronomical observations. A remaining problem - the difficulty of cutting grooves on those materials - has recently been overcome by the nano precision fly-cutting technique. Therefore, we conclude that CVD-ZnS and CVD-ZnSe are best suited as materials for immersion gratings in the sNIR region. We believe that ZnS and ZnSe immersion gratings for astronomical observation can be technically realized.

Acknowledgments

We would like to thank A. Tokunaga for fruitful suggestions and comments throughout this study. Most measurements were carried out at the Advanced Technology Center (ATC) of the National Astronomical Observatory of Japan (NAOJ). We feel most grateful to all the staff of ATC, especially to K. Mitsui for supporting our measurements kindly. This work was supported by KAKENHI (16684001) Grant-in-Aid for Young Scientists (A) and KAKENHI (20340042) Grant-in-Aid for Scientific Research (B) by the Japan Society for the Promotion of Science (JSPS). It is also supported by the Grant for Collaborative Basic Development (FY2007) and General Funds by NAOJ, and the Grant for the Space Instrument Basic Development (FY2007) by Institute of Space and Astronautical Science (ISAS), Japan Aerospace Exploration Agency (JAXA). A portion of this work was performed under the auspices of the U.S. Department of Energy by Lawrence Livermore National Laboratory under Contract DE-AC52-07NA27344. Authors Kondo and Yasui are financially supported by the JSPS fellowship.

-
- [1] E. Hulthén and H. Heuhaus, *Nature* **173**, 442 (1954).
 - [2] C. G. Wynne, *Optics Communications* **73**, 419 (1989).
 - [3] C. G. Wynne, *Optics Communications* **75**, 1 (1990).
 - [4] C. G. Wynne, *Optics Communications* **77**, 355 (1990).
 - [5] R. Szumski and D. D. Walker, *Mon. Not. R. Astron. Soc.* **302**, 139 (1999).
 - [6] D. Lee and J. R. Allington-Smith, *Mon. Not. R. Astron. Soc.* **312**, 57 (2000).
 - [7] J. P. Marsh, D. J. Mar, and D. T. Jaffe, *Appl. Opt.* **46**, 3400 (2007).
 - [8] S. S. Vogt, S. L. Allen, B. C. Bigelow, L. Bresee, B. Brown, T. Cantrall, A. Conrad, M. Couture, C. Delaney, H. W. Epps, et al., in *Instrumentation in Astronomy VIII*, edited by Crawford, D. L. and Craine, E. R. (1994), vol. 2198 of *Proc. SPIE*, p. 362.
 - [9] S. D'Odorico, S. Cristiani, H. Dekker, V. Hill, A. Kaufer, T. Kim, and F. Primas, in *Discoveries and Research Prospects from 8- to 10-Meter-Class Telescopes*, edited by Bergeron, J. (2000), vol. 4005 of *Proc. SPIE*, pp. 121–130.
 - [10] K. Noguchi, W. Aoki, S. Kawanomoto, H. Ando, S. Honda, H. Izumiura, E. Kambe, K. Okita, K. Sadakane, B. Sato, et al., *The Publications of the Astronomical Society of Japan* **54**, 855 (2002).
 - [11] H.-U. Kaeufl, P. Ballester, P. Biereichel, B. Delabre, R. Donaldson, R. Dorn, E. Fedrigo, G. Finger, G. Fischer, F. Franza, et al., in *Ground-based Instrumentation for Astronomy*, edited by Moorwood, A. F. M. and Iye, M. (2004), vol. 5492 of *Proc. SPIE*, pp. 1218–1227.
 - [12] H. Dekker, in *Instrumentation for Ground-Based Optical Astronomy, Present and Future*, edited by L. B. Robinson (1988), pp. 183–+.

- [13] G. R. Wiedemann, H. H. Dave, and D. E. Jennings, in *Infrared Detectors and Instrumentation*, edited by Fowler, A. M. (1993), vol. 1946 of *Proc. SPIE*, pp. 622–628.
- [14] T. A. Sebring, G. Moretto, F. N. Bash, F. B. Ray, and L. W. Ramsey, in *Proceedings of the Backaskog workshop on extremely large telescopes*, edited by T. Andersen, A. Ardeberg, and R. Gilmozzi (2000), p. 53.
- [15] G. Monnet and R. Gilmozzi, in *The Scientific Requirements for Extremely Large Telescopes*, edited by P. Whitelock, M. Dennefeld, and B. Leibundgut (2006), vol. 232 of *IAU Symposium*, pp. 429–431.
- [16] R. Gilmozzi and J. Spyromilio, *The Messenger* **127**, 11 (2007).
- [17] P. Klocek, ed., *Handbook of Infrared Optical Materials* (Marcel Dekker Inc., New York, 1991).
- [18] N. C. Fernelius, G. A. Graves, and W. L. Knecht, in *Emerging Optical Materials*, edited by S. Musikan (1981), vol. 297 of *Presented at the Society of Photo-Optical Instrumentation Engineers (SPIE) Conference*, p. 188.
- [19] C. A. Klein, R. P. Miller, and D. L. Stierwalt, *Appl. Opt.* **33**, 4304 (1994).
- [20] D. T. Marple, *Phys.Rev.* **150**, 728 (1966).
- [21] P. Klocek, J. T. Hoggins, T. A. McKenna, J. M. Trombetta, and M. W. Boucher, in *Society of Photo-Optical Instrumentation Engineers (SPIE) Conference Series*, edited by J. W. Tuttle (1991), vol. 1498 of *Presented at the Society of Photo-Optical Instrumentation Engineers (SPIE) Conference*, pp. 147–157.
- [22] G. G. Macfarlane and V. Roberts, *Phys.Rev.* **98**, 1865 (1955).
- [23] A. Hordvik and L. Skolnik, *Appl. Opt.* **16**, 2919 (1977).
- [24] M. Wakaki, K. Kudo, and T. Shibuya, *Physical Properties and Data of Optical Materials* (CRC Press, New York, 2007).
- [25] D. E. Aspnes and A. A. Studna, *Phys. Rev. B* **27**, 985 (1983).
- [26] J. C. Richter, C. R. Poznich, and D. W. Thomas, in *Window and Dome Technologies and Materials II*, edited by P. Klocek (1990), vol. 1326 of *Presented at the Society of Photo-Optical Instrumentation Engineers (SPIE) Conference*, pp. 106–119.
- [27] D. C. Harris and E. A. Anagnostakis, *Materials for Infrared Windows and Domes* (SPIE Optical Engineering Press, Bellingham, 1999).
- [28] A. Hordvik and H. Schlossberg, *Appl. Opt.* **16**, 101 (1977).
- [29] G. G. Macfarlane and V. Roberts, *Phys.Rev.* **97**, 1714 (1955).
- [30] H. Y. Fan and M. Becker, *Phys.Rev.* **78**, 178 (1950).
- [31] L. Tsang, J. A. Kong, and K.-H. Ding, *Scattering of Electromagnetic Waves, Theories and Applications* (Hoboken, NJ, John Wiley & Sons, Inc., 2000).
- [32] R. W. Wilson and C. R. Jenkins, *MNRAS* **278**, 39 (1996).
- [33] P. J. Kuzmenko, L. M. Little, P. J. Davis, and S. L. Little, in *IR Space Telescopes and Instruments*, edited by J. C. Mather (2003), pp. 1179–1190.
- [34] P. J. Kuzmenko, P. J. Davis, S. L. Little, and L. C. Hale, in *Optomechanical Technologies for Astronomy* (2006), vol. 6273 of *Presented at the Society of Photo-Optical Instrumentation Engineers (SPIE) Conference*.
- [35] P. J. Kuzmenko, P. J. Davis, S. L. Little, L. M. Little, and J. V. Bixler, in *Optomechanical Technologies for Astronomy* (2006), vol. 6273 of *Presented at the Society of Photo-Optical Instrumentation Engineers (SPIE) Conference*.
- [36] P. J. Kuzmenko, S. L. Little, Y. Ikeda, and N. Kobayashi, in *Advanced Optical and Mechanical Technologies in Telescopes and Instrumentation. Proceedings of the SPIE, 7018-181* (2008), vol. 7018 of *Presented at the Society of Photo-Optical Instrumentation Engineers (SPIE) Conference*.
- [37] Y. Ikeda, N. Kobayashi, P. Kuzmenko, S. Little, C. Yasui, S. Kondo, A. Minami, and K. Motohara, in *Advanced Optical and Mechanical Technologies in Telescopes and Instrumentation. Proceedings of the SPIE, 7018-183* (2008), vol. 7018 of *Presented at the Society of Photo-Optical Instrumentation Engineers (SPIE) Conference*.
- [38] P. J. Dean and D. G. Thomas, *Phys.Rev.* **150**, 690 (1966).
- [39] The absorption coefficients plotted in Fig.2 are obtained from a polycrystalline GaP [21]. Single crystal GaP is free from bulk scattering at grain boundaries. Measurements on the optical transmission of ultrapure single crystal GaP indicate the possibility of low absorption loss ($\alpha_{\text{abs}} \sim 0.01 \text{ cm}^{-1}$) down to the short wavelength cut-off at $\lambda \sim 0.57 \mu\text{m}$ [38]. Their crystals were grown by a special modified wet-hydrogen transport process. Unfortunately most commercially available gallium phosphide is grown by a liquid encapsulated Czochralski (LEC) process that yields much poorer short wavelength transmission as shown in Fig.2. Additionally, the LEC material is quite expensive. Further study on the availability of ultra high purity material should be done.

TABLE I: The attenuation coefficients of CVD-ZnS, CVD-ZnSe, Si, and GaAs

λ (μm)	CVD-ZnS	CVD-ZnSe	Si	GaAs
	α_{att} (cm^{-1})			
0.72	3.07E-02	4.42E-02		
0.74	2.58E-02	4.15E-02		
0.76	2.53E-02	3.93E-02		
0.78	2.47E-02	3.72E-02		
0.80	2.39E-02	3.55E-02		
0.82	2.30E-02	3.39E-02		
0.84	2.27E-02	3.26E-02		
0.86	2.22E-02	3.10E-02		
0.88	2.33E-02	2.85E-02		
0.89				3.49E+01
0.90	2.10E-02	2.78E-02		8.59E+00
0.91				2.96E+00
0.92	1.96E-02	2.86E-02		2.21E+00
0.94	1.94E-02	2.61E-02		1.89E+00
0.96	1.87E-02	2.54E-02		1.68E+00
0.98	1.81E-02	2.41E-02		1.53E+00
1.00	1.77E-02	2.33E-02		1.39E+00
1.02	1.71E-02	2.24E-02		1.26E+00
1.04	1.67E-02	2.17E-02		1.15E+00
1.06	1.59E-02	2.08E-02		1.06E+00
1.08	1.58E-02	1.99E-02		9.74E-01
1.10	1.56E-02	1.95E-02		8.72E-01
1.12	1.55E-02	1.88E-02		7.66E-01
1.14	1.50E-02	1.82E-02		6.28E-01
1.16	1.48E-02	1.76E-02		5.16E-01
1.18	1.43E-02	1.67E-02		4.04E-01
1.20	1.41E-02	1.64E-02	1.80E-02	3.06E-01
1.21			1.37E-02	
1.22	1.38E-02	1.58E-02	7.25E-03	2.21E-01
1.23			4.64E-03	
1.24	1.35E-02	1.51E-02	2.74E-03	1.67E-01
1.25			1.39E-03	
1.26	1.31E-02	1.48E-02	7.50E-04	1.26E-01
1.27			5.63E-04	
1.28	1.29E-02	1.44E-02	6.75E-04	9.54E-02
1.30	1.28E-02	1.38E-02	6.63E-04	7.20E-02
1.32	1.25E-02	1.35E-02	7.13E-04	
1.34	1.19E-02	1.27E-02	8.00E-04	
1.36	1.16E-02	1.22E-02	5.25E-04	
1.38	1.16E-02	1.14E-02	6.25E-04	
1.40	1.13E-02	1.16E-02	5.25E-04	
1.42	1.12E-02	1.14E-02	5.75E-04	
1.44	1.10E-02	1.11E-02	1.06E-03	
1.46	1.07E-02	1.09E-02	1.18E-03	
1.48	1.06E-02	1.03E-02	9.00E-04	
1.50	1.05E-02	1.02E-02	1.14E-03	
1.52	1.05E-02	9.81E-03	1.09E-03	
1.54	1.03E-02	9.46E-03	1.19E-03	
1.56	9.75E-03	9.31E-03	9.00E-04	
1.58	9.79E-03	9.23E-03	1.53E-03	
1.60	9.46E-03	8.31E-03		